



Porphyrinic MOF Film for Multifaceted Electrochemical Sensing

Zhenyu Zhou, Soumya Mukherjee, Shujin Hou, Weijin Li,* Martin Elsner, and Roland A. Fischer*

Abstract: Electrochemical sensors are indispensable in clinical diagnosis, biochemical detection and environmental monitoring, thanks to their ability to detect analytes in real-time with direct electronic readout. However, electrochemical sensors are challenged by sensitivity—the need to detect low concentrations, and selectivity—to detect specific analytes in multi-component systems. Herein, a porphyrinic metal-organic framework (PP-MOF), Mn-PCN-222 is deposited on a conductive indium tin oxide (ITO) surface. It affords Mn-PCN-222/ITO, a versatile voltammetric sensor able to detect redox-active analytes such as inorganic ions, organic hazardous substances and pollutants, including nitroaromatics, phenolic and quinone-hydroquinone toxins, heavy metal ions, biological species, as well as azo dyes. As a working electrode, the high surface area of Mn-PCN-222/ITO enables high currents, and therefore leverages highly sensitive analysis. The metalloporphyrin centre facilitates analyte-specific redox catalysis to simultaneously detect more than one analyte in binary and ternary systems allowing for detection of a wide array of trace pollutants under real-world conditions, most with high sensitivity.

Introduction

Electrochemical sensing stems from changes in the detectable electric signal caused by the interactions between electrode and specific analytes. Thanks to its advantages, such as quick response, high efficiency, simple operation, and

analyte-specific redox potentials that open specific windows for detection, electrochemical sensors have spurred considerable research interest and have been widely used in clinical diagnosis, biochemistry and environmental monitoring.^[1] Besides potentiometric sensors, voltammetric (= Volt-/ Amperometric) sensors are the most common kind. Here analyte-specific redox reactions are detected by measuring the corresponding electrical current in response to changes in the applied electrochemical potential.^[1b,2] This has propelled cyclic voltammetry (CV) as a front-runner for sensing redox-active analytes. Here, the applied potential at the working electrode is varied back and forth at a certain scan rate over a specific potential range. By plotting the current response versus the applied potential, a cyclic voltammogram trace is obtained,^[3] which is symmetric in the case of reversible redox reactions at the electrode surface and non-symmetric otherwise. Despite such successful technological examples as the Clark electrode for detection of oxygen,^[4] the high sensitivity and universality of electrochemical sensors (i.e., the ability to detect a wide range of analytes such as organic pollutants, heavy ions, biological markers and azo dyes) remain unmet challenges until today.

Metal-organic frameworks (MOFs), composed of organic linkers and inorganic metal nodes (or clusters), have drawn enormous attention due to their well-defined porous structures with high surface areas, good stability and tailored functionalities.^[5] These features lead to an increased propensity for the analytes to get concentrated and to expedite rapid mass transfer of the analytes across a large surface area. This in turn amplifies the voltammetric current as a characteristic signal response and thereby enhances sensitivity, making MOFs promising for electrochemical sensing.^[1a,6] On the other hand, thanks to their π -conjugated macrocyclic structures, porphyrins and metalloporphyrins demonstrate good electron transfer and selective redox catalytic properties, thus befitting to electrochemically sense several target analytes.^[7]

Considering these advantages of MOFs and porphyrins, we develop porous porphyrinic MOFs (PP-MOFs) treating these as molecular building blocks. In the pursuit of electrochemical sensing, PCN-222 (PCN, porous coordination network), a prototypical PP-MOF constructed from Zr₆ cluster and tetrakis(4-carboxyphenyl)-porphyrin (TCPP) ligand is used. PCN-222 features ultrahigh surface areas (>2000 m² g⁻¹).^[8] Its 1D hexagonal mesopores (\approx 3.0 nm) replete with porphyrin sites (Figure 1 a) endow it as a potent lead to enable electrocatalytic sensing.^[9] In pursuit of electrochemical applications, integration of PP-MOFs onto solid surfaces in the form of films is a prerequisite that we achieve herein.^[10]

[*] Z. Y. Zhou, Dr. S. Mukherjee, Dr. W. J. Li, Prof. R. A. Fischer
Chair of Inorganic and Metal-Organic Chemistry, Department of
Chemistry, Technische Universität München
Lichtenbergstraße 4, 85748 Garching b. München (Germany)
E-mail: wj.li@tum.de
roland.fischer@tum.de

S. J. Hou
Physics of Energy Conversion and Storage, Physic-Department,
Technische Universität München
James-Franck-Str. 1, 85748 Garching b. München (Germany)
Prof. M. Elsner
Chair of Analytical Chemistry and Water Chemistry, Technische
Universität München, Department of Chemistry
Lichtenbergstraße 4, 85748 Garching b. München (Germany)

Supporting information and the ORCID identification number(s) for the author(s) of this article can be found under:
<https://doi.org/10.1002/anie.202107860>.

© 2021 The Authors. Angewandte Chemie International Edition published by Wiley-VCH GmbH. This is an open access article under the terms of the Creative Commons Attribution Non-Commercial NoDerivs License, which permits use and distribution in any medium, provided the original work is properly cited, the use is non-commercial and no modifications or adaptations are made.

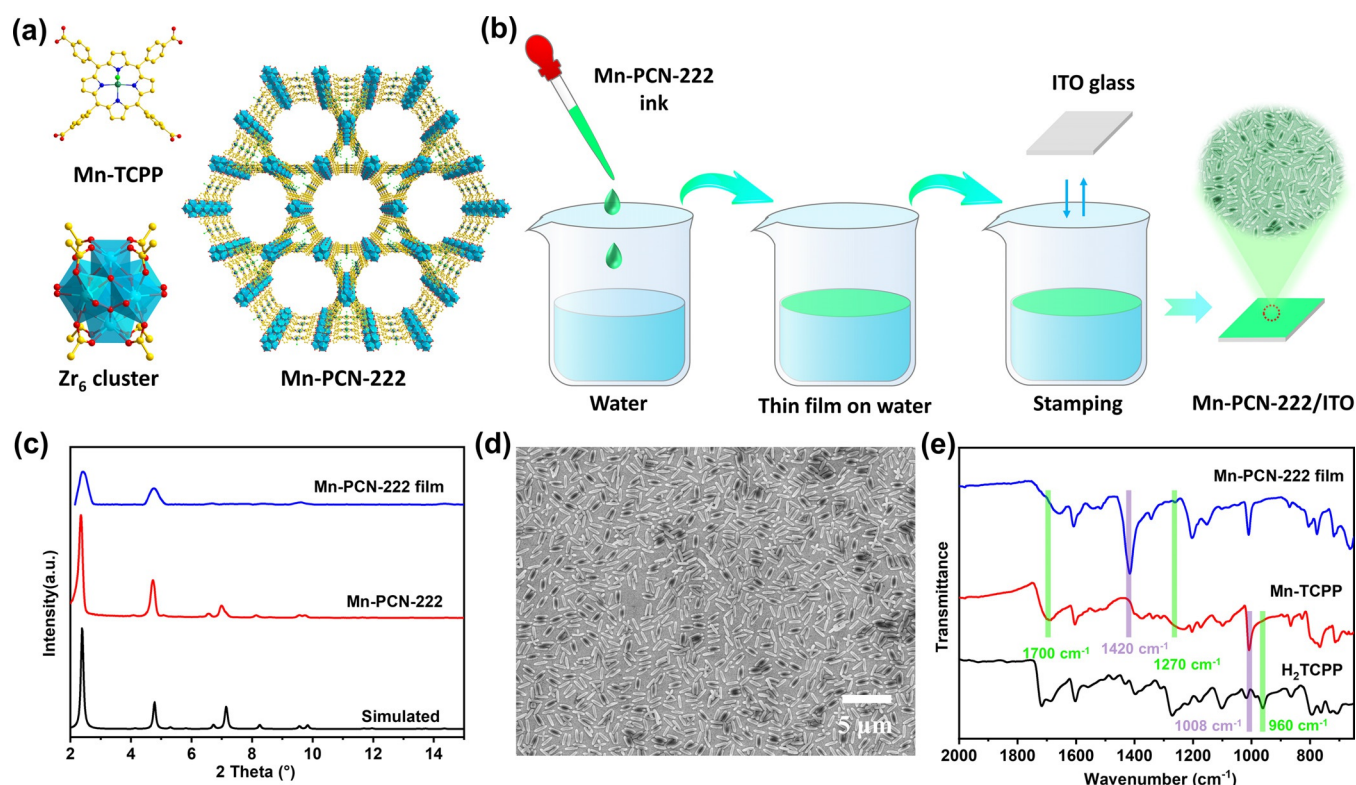


Figure 1. (a) Structures of the building blocks: Mn-TCPP ligand and Zr_6 cluster sustaining Mn-PCN-222; the framework structure of Mn-PCN-222 with 1D triangular microchannels and hexagonal mesochannels. H atoms are omitted for clarity. Color Scheme: C, yellow; O, red; N, blue; Cl, olive green and Mn, cyan. (b) Schematic illustration of the modular assembly driven synthetic route leading to a Mn-PCN-222/ITO electrode. (c) Simulated and experimental PXRD patterns of the bulk Mn-PCN-222 and GIXRD patterns of the Mn-PCN-222 film fabricated by modular assembly. (d) SEM images of the Mn-PCN-222 film casted on ITO glass. (e) ATR-IR spectra of free H_2 TCPP ligand, Mn-TCPP ligand and Mn-PCN-222 film.

Recently, Mn-PCN-222 modified with poly-glutamic acid has been utilized earlier as an electrochemical H_2O_2 sensor.^[9b] Nevertheless, the suitability of Mn-PCN-222 rests upon rationally combining metalloporphyrin redox sites with porosity, each enabling facile electron transfer and analyte transport. This, in unison, leads to a miscellany of sensing performances while detecting several analytes. Low detection limits are manifested herein, that cover both inorganic substrates and organic pollutants. Also, critical analysis of such a multifaceted detection process remains an uncharted territory. Herein, we forge ahead with our detailed electrochemical studies to fill this knowledge gap by selecting to study Mn-PCN-222 as a versatile sensor.

In this study, a facile and straightforward modular assembly technique for liquid-phase depositing of Mn-PCN-222 (manganese metalloporphyrin) film on conductive indium tin oxide (ITO) glass leads us to fabricate the Mn-PCN-222/ITO electrode (Figure 1b).^[8b,11] Herein, solvothermally synthesized PP-MOF nanoparticles (NPs) serve as thin film precursors. Thanks to hydrophobicity, these PP-MOF NPs spontaneously spread out as a thin film on water, from which they are easily transferred to the substrate. This simple stamping results in a very homogeneous thin film of assembled NPs. Overall, our observations introduce modular assembly as a reliable and efficient way of preparing PP-MOF film electrodes for multifunctional electrochemical sensors.

To the best of our knowledge, this is the first report of an electrochemical sensor built from modular assembly.

Results and Discussion

Powder X-ray diffraction (PXRD) patterns of the Mn-PCN-222 powder and its film obtained via modular assembly are shown in Figure 1c. These diffraction patterns are found to be in good agreement with the simulated XRD profile, suggesting bulk phase purity of the crystallized samples and confirming that the obtained thin film solely comprise the Mn-PCN-222 crystallites.^[8,12] Scanning electron microscopy (SEM) of an Mn-PCN-222 film-modified ITO electrode shows the film to be composed of rod-shaped Mn-PCN-222 crystallites (length $\approx 1 \mu m$) evenly dispersed on the ITO surface (Figure 1d). In principle, if the properties of building blocks are synergized, such a uniform coverage of Mn-PCN-222 crystallites on the conductive surface of ITO should indeed lead to an efficient electrochemical sensor.^[10b] Energy-dispersive X-ray spectroscopy (EDX) confirms a uniform distribution of Mn elements across the Mn-PCN-222 thin film (Figure S1). Attenuated total reflection infrared spectroscopy (ATR-IR) spectra and ultraviolet-visible spectroscopy (UV/Vis) spectra are recorded to further identify the compositions of the prepared Mn-PCN-222 film (Figures 1e and S2). In

contrast to the free H₂TCPP ligand, the metallisation of Mn-TCPP ligand is evidenced by disappearance of the N-H stretching vibration at 960 cm⁻¹ and appearance of a new peak at 1008 cm⁻¹ assigned to Mn–N bonds.^[8b,13] The latter signature is also found in the Mn-PCN-222 film (Figure 1 e). This is well aligned with the EDX and UV/Vis spectra (Figures S1 and S2). Moreover, compared to the spectrum of Mn-TCPP, Mn-PCN-222 films exhibit an absence of characteristic peaks around 1700 cm⁻¹ (C=O bonds) and 1270 cm⁻¹ (C–O bonds) whereas strong peaks at 1420 cm⁻¹ (COO symmetric stretch bonds) appear, reflective of the carboxyl group coordinating to the Zr₆ centres in Mn-TCPP.^[8b,14] To verify the loading of Mn-PCN-222 onto the ITO electrode each time, UV-vis spectra of 10 independent samples are investigated and the absorbances at 465 nm are noted (Table S1).^[13a] An average absorbance of 0.1421 a.u. (Figure S3) is observed, whereas its excellent reproducibility is evidenced by the low relative standard deviation (RSD) of just 3.0%. The porosity of bulk Mn-PCN-222 is examined by N₂ adsorption experiments and the typical type-IV isotherm is accompanied by a steep rise at ca. $P/P_0 = 0.3$, suggesting both micro and mesoporosity (Figure S4). The pore size distribution profile indicates two types of pores with sizes of ≈ 1.3 nm and ≈ 3.0 nm, assigned to the coexistence of 1D triangular microchannels and hexagonal mesochannels, respectively in the framework structure (Figure 1 a).^[8a] Applying Rouquerol criteria to the 77 K N₂ isotherm, the Brunauer-Emmett-Teller (BET) surface area is evaluated as high as 2013 m²g⁻¹.^[15] A methanol sorption isotherm recorded on the environmentally controlled quartz crystal microbalance (BEL-QCM) confirms the high porosity of film-deposited NPs (Figure S5). The large 1D mesochannels and high surface area, in principle, should prove beneficial to enable rapid analyte aggregation and mass transport.^[8a,9a,b]

After characterizing the prepared Mn-PCN-222 film, as a proof of concept, we begin to critically examine their functions as electrochemical sensors. Before testing any other hazardous inorganic and organic substances, one of the most common representatives of nitroaromatic compounds, nitrobenzene (NB), is chosen as a model toxin. Chasing after CV based sensing, this compound allows us to optimize the critical parameters, e.g., scan rate, pH, accumulation time. It also offers to study selectivity, stability, recyclability and reproducibility, in which the currents of CV reduction peaks correspond to signal readouts.

Both toxicity and carcinogenicity aspects are well-documented for nitroaromatics, particularly nitrobenzene (NB) and their derivatives. These can pose threats to human health and the environment even at low concentrations of ca. 2 mgL⁻¹.^[16] Rapid and efficient detection of NB in water is, therefore, a matter of high societal and environmental relevance. To begin with, as an electrochemical sensor for NB detection, the Mn-PCN-222/ITO electrode is studied and the corresponding sensitivity and selectivity of detection are determined. In the absence of NB, a pair of redox peaks are observed on the CV curve at ca. -0.45 V and -0.32 V (Figure 2 a), corresponding to the reversible couple of Mn^{III}/Mn^{II} on Mn-PCN-222.^[17] The Mn-PCN-222/ITO-modified electrode exhibited a sharp, irreversible reduction peak at

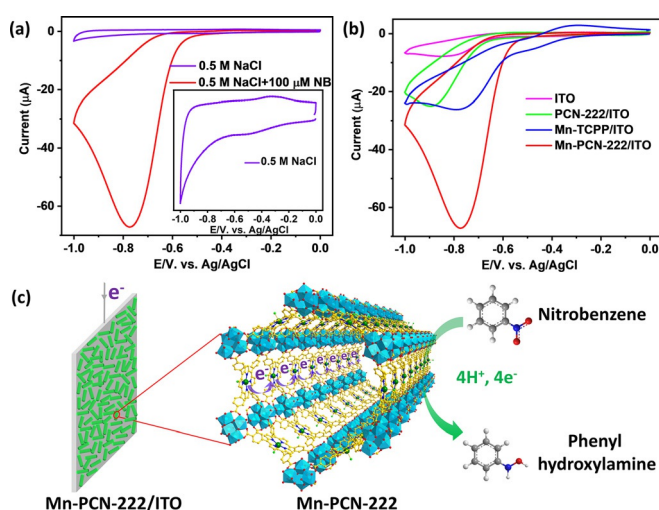


Figure 2. (a) CV profiles of the Mn-PCN-222/ITO electrode in 0.5 M NaCl solution in the presence or absence of 100 μM NB at a scan rate of 50 mVs⁻¹. Inset: an enlarged CV curve obtained in the absence of 100 μM NB for comparative clarity. (b) CV curves recorded on different electrodes targeting the reduction of 100 μM NB. (c) Schematic illustration of the plausible mechanism of NB reduction on the Mn-PCN-222/ITO electrode.

-0.77 V in the presence of 100 μM NB. This could be attributed to the direct reduction of NB to phenylhydroxylamine in neutral medium, concomitant with the transfer of four electrons and protons (Figure 2 c).^[16b,c] Relying upon this reduction, the modified electrode shows potential as an electrochemical sensor for NB detection. The detailed process and putative mechanisms for the electrocatalytic NB reduction on the Mn-PCN-222/ITO can be described as follows: first, the large surface area of Mn-PCN-222 and the highly π -conjugated porphyrin ring (π - π interactions with NB) contribute to the aggregation of NB molecules; on top of this, the porphyrin ligands feature intrinsic redox activity, which would contribute to the electrochemical sensing of redox-active NB analytes; under an external voltage, the Mn^{III} porphyrin centres of Mn-PCN-222 are reduced to Mn^{II} porphyrins state and serve as electron donors. Meanwhile, thanks to the strong electron-withdrawing nature of the nitro group, NB acts as an excellent electron acceptor, thus affording an electron donor-acceptor (EDA) system formed between the porphyrin centres and the NB molecules; this EDA system facilitates sequential electron transfer to the nitro group, followed by protonation, thereby culminating in the reduction of NB.^[7a,16c,18]

To further evaluate NB reduction performances of the Mn-PCN-222/ITO electrode and to rationally compare, a) bare ITO; b) non-metallated PCN-222/ITO; and c) Mn-TCPP/ITO electrodes are also prepared separately. As shown in Figure 2 b, the bare ITO shows a weak current response with -0.06 V negative shifts for NB compared to that of Mn-PCN-222/ITO electrode, clearly revealing its poor response as a redox catalyst towards NB. Regarding the as-prepared modified electrodes, the Mn-PCN-222/ITO electrode also exhibits superior electrochemical behaviour. A three-fold increase in reduction current is observed against the non-

metallated PCN-222/ITO electrode. The better electrocatalytic activity towards NB is attributed to the faster charge hopping and improved redox activity after coordination of Mn^{III} to the porphyrin centres (Figure 2c).^[9d,10c,19] Moreover, among the metallated M-PCN-222 (M = Mn, Fe, Co, Cu, and Zn) variants, Mn-PCN-222/ITO ranks as the front runner for NB reduction (Figures S6–S8). Meanwhile, a Mn-TCPP/ITO electrode is also prepared for comparison. Quantified by UV/Vis, the catalytically active Mn-TCPP are equally loaded on both Mn-TCPP/ITO and Mn-PCN-222/ITO electrodes (Figure S9). The superiority of Mn-PCN-222 with high surface area, large 1D mesochannels and ordered accessible active sites is evidenced by the comparative examination of Mn-TCPP/ITO electrodes (Figure 2b).

The effect of scan rate (ranging from 30 to 150 mV s^{-1}) towards NB reduction is assessed by cyclic voltammetry (Figure S10). The reduction peak current increased linearly with respect to the square root of scan rate with a correlation coefficient R^2 of 0.9996. This suggests a typical diffusion-controlled process to drive the electrochemical reduction of NB at the modified electrode.^[16b-d] Moreover, the electron transfer number for cathodic NB reduction is estimated as 3.8 according to Laviron's equation,^[20] suggesting a 4 electrons transfer process. Conversely, the chronoamperometric response of Mn-PCN-222/ITO towards different NB concentrations reveals the diffusion coefficient for NB to be $6.178 \times 10^{-6} \text{ cm}^2 \text{ s}^{-1}$ based on Cottrell's equation (Figure S11).^[9a,c,d]

pH is another key parameter that may profoundly influence the performance of a voltammetric sensor, i.e., the respective redox potential and the kinetics of the redox reaction. Herein, CV curves of Mn-PCN-222/ITO electrode are recorded across different pH (5 to 9) (Figure S12). CV profiles recorded at a relatively high H^+ concentration (pH 5) exhibit an increased reduction current at -1.0 V , corresponding to a side reaction of hydrogen evolution reaction (HER). Concurrently, during reduction, a low H^+ concentration (at pH 9) hinders the subsequent NB reduction due to the increased difficulty in protonation. In comparison with solutions of varying pH, the maximum peak-current response towards NB reduction is found to be achieved at pH 7.^[16b-d] Hence, pH 7 is concluded to be the optimum pH for detecting NB on the Mn-PCN-222/ITO electrode. Moreover, with increasing pH, the reduction peak potential (E_p) exhibits a linear shift to the negative end with the corresponding equation of $E_p^{\text{V}} = -0.0581 \text{ pH} - 0.368$. The slope of 58.1 mV pH^{-1} is found in close agreement with the theoretical value, 59 mV pH^{-1} , indicating that an equal number of protons and electrons are transferred during NB reduction.^[21] Simply put, the pH dependence of electrochemical behaviour reflects the influence of H^+ on NB reduction while studying the electrode, which in turn corresponds to the mechanism of NB reduction.^[16b-d]

The influence of another parameter, *viz.* accumulation time, is also investigated by altering the accumulation time just before measuring the cyclic voltammograms (Figure S13). Under a low NB concentration of $10 \mu\text{M}$, the CV response currents increase as a function of the time of accumulation. This is attributed to the increased amount of NB molecules aggregated on the Mn-PCN-222/ITO electrode. Thereafter,

the current peak values remain nearly constant after an accumulation time $> 90 \text{ s}$, presumably due to NB saturation of the modified electrode under a dynamic equilibrium. Interestingly, a rapid saturation is achieved at a high NB concentration ($100 \mu\text{M}$). This could be ascribed to the high surface area and large 1D mesochannels of Mn-PCN-222, leading to rapid analyte aggregation and mass transport.^[8a,9b] According to these results in Figure S13, 90 s is selected as the optimum accumulation time for further investigation.

The feasibility of Mn-PCN-222/ITO electrode for NB detection is confirmed under optimized conditions with the addition of different concentrations of NB (Figure 3a; for zoomed views of the low concentrations, see Figure S14). Notably, the corresponding reduction peak currents (I) increased linearly with the increase in NB concentration (c) ranging from 0.08 up to $700 \mu\text{M}$ with high correlation coefficients ($R^2 > 0.999$). According to the criterion of United States of Environmental Protection Agency (USEPA), the acceptable limit of NB in water is 2 mg L^{-1} ($16.25 \mu\text{M}$),^[16a,c] falling within the detectable range of the modified electrode, thus suggesting its potential for NB detection. In addition, the sensitivity is determined to be $0.6479 \mu\text{A} \mu\text{M}^{-1} \text{ cm}^{-2}$ (0.08 – $100 \mu\text{M}$) and $0.4468 \mu\text{A} \mu\text{M}^{-1} \text{ cm}^{-2}$ (100 – $700 \mu\text{M}$), respectively. The slight difference of sensitivity is likely to be an outcome of the following concentration-guided factors: a) the abundance of catalytic sites implies their easy accessibility for the absorbed NB molecules at low concentrations; b) nevertheless at higher concentrations, these sites become sequestered owing to saturation with NB, thus compromising the sensitivity.^[9a-c] The limit of detection (LOD) is calculated as low as $0.03 \mu\text{M}$ ($3 \times S_b/\text{slope}$, Figure S15, Table S2). Compared to the previously reported modified electrodes for NB detection, the proposed Mn-PCN-222/ITO electrode sets a benchmark analytical response towards NB in terms of a wide linear response and low LOD (Table S3). Its electrocatalytic activity towards NB detection stands out, and can be correlated to its large surface area, expedited preconcentration, rapid mass transport and high density of the accessible, ordered active sites in Mn-PCN-222.^[8a,9a,b]

We evaluated the selectivity of the Mn-PCN-222/ITO electrode towards NB ($50 \mu\text{M}$) in the presence of 10 fold molar excess of other typical interferents (Figure S16). It can be seen that common metal ions and biological species only induce negligible interference ($< 2\%$) whereas phenolic compounds, quinone and benzene derivatives only trigger measly effects ($< 4\%$) on the NB detection performance. These results indicate the potential of the modified electrodes for selectively detecting NB, even in the presence of an excess of these potentially interfering species.

To further confirm practical viability, the modified electrode is employed to detect NB in real water samples (tap water and river water) with addition of NB of different concentrations ($10 \mu\text{M}$, $20 \mu\text{M}$ and $30 \mu\text{M}$) and analyzed by cyclic voltammograms (Table S4). The Mn-PCN-222/ITO electrode featured excellent recoveries (the percentages of measured concentrations to the corresponding added concentrations) towards NB detection (96.2 to 102.5%) in real samples, suggestive of its suitability as NB sensor to detect water contamination.^[16b,c]

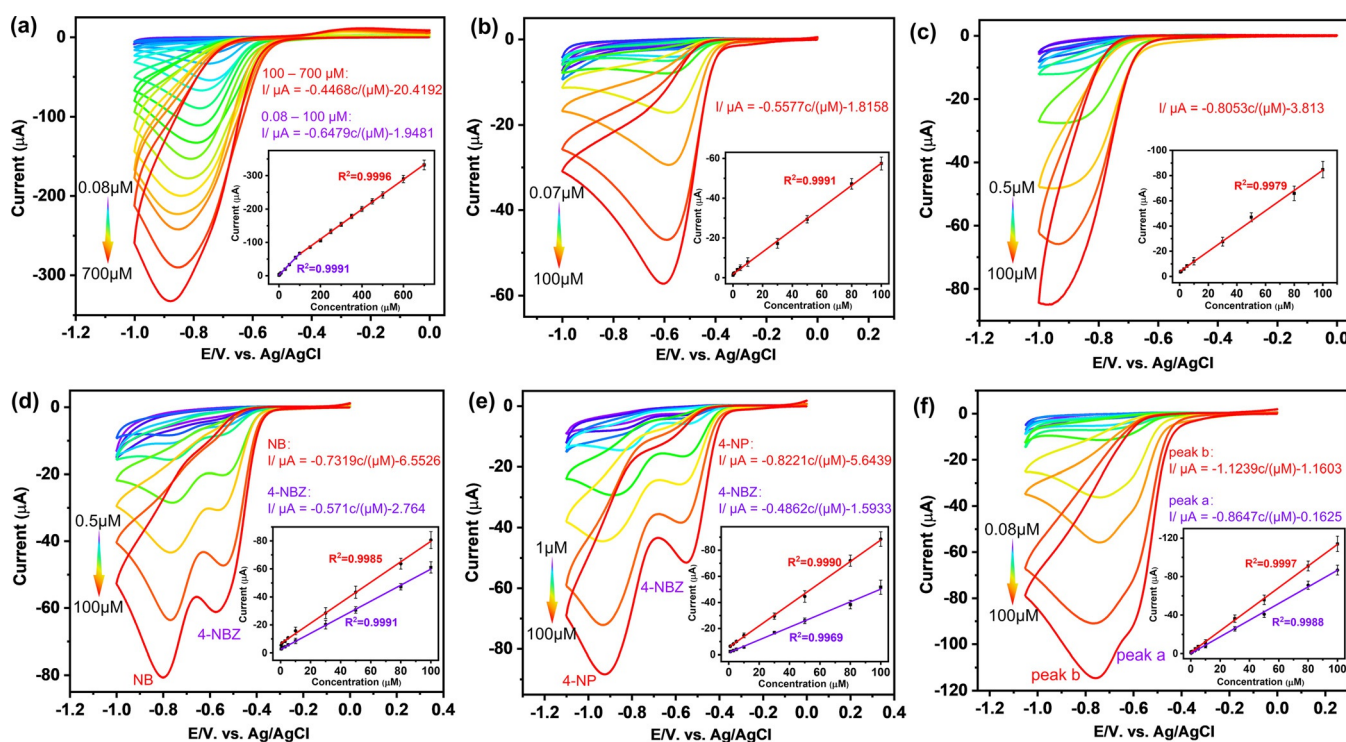


Figure 3. CV curves of the Mn-PCN-222/ITO electrode towards the detection of (a) NB, (b) 4-NBZ, (c) 4-NP, (d) NB and 4-NBZ, (e) 4-NP and 4-NBZ, (f) 1,3-DNB at different concentrations; inset shows linear trend of the peak current versus concentration of corresponding analytes.

Material stability, recyclability and reproducibility are important parameters for electrochemical sensors. Mn-PCN-222/ITO exhibits excellent stability substantiated by the retention of nearly 97.3% of its initial response after 30 days (Figure S17). The high stability originates from the stable Zr_6 cluster and strong chelating effect between Mn^{III} and the porphyrins.^[8a,9b,c] The electrode also shows good recyclability with a RSD of 4.98% ($< 5\%$) for 40 measurement cycles (Figure S18). Meanwhile, a comparison of the XRD patterns, SEM images, UV/Vis spectra and Raman spectra on the modified electrodes reveals identical crystalline features and morphologies, changeless coating condition as well as same molecular structures before and after consecutive detection measurements, indicating their excellent electrochemical and mechanical stability (Figures S19–S23). Furthermore, 10 independent Mn-PCN-222/ITO electrodes are examined. A RSD of 2.67% ($< 5\%$) (Table S5) suggests outstanding reproducibility of the modified electrode.

Aligned with the observations made in our foregoing experiments, the feasibility of Mn-PCN-222/ITO for NB detection becomes clear. To verify the versatility of the proposed modified electrode, electrochemical detection of other nitroaromatic compounds (NACs), *viz.* 4-nitrobenzaldehyde (4-NBZ), 4-nitrophenol (4-NP), 1,3-dinitrobenzene (1,3-DNB) are investigated in individual and/or simultaneous modes (Figures 3b–f). Although a reduction peak appears due to the presence of a nitro group, the peak potentials for 4-NBZ and 4-NP register clear shifts compared to that of NB due to the withdrawal or donation of electron density at the nitro group by different substituent groups at the NAC rings.^[16d,22] The -CHO group in 4-NBZ withdraws the electron

density from the aromatic ring, then resulting in an electron-deficient nitro group that is more easily reduced. Therefore, a positive shift of reduction potential is observed for 4-NBZ (−0.60 V). On the contrary, the electron-donating group -OH in 4-NP facilitates a negative shift of the reduction potential to −0.95 V. As shown in Figures 3b,c, the Mn-PCN-222/ITO exhibits linear responses to 4-NBZ (0.07–100 μM) and 4-NP (0.5–100 μM) with high correlation coefficients (0.9991 and 0.9979, respectively). The LOD for the detection of 4-NBZ and 4-NP detection are 0.030 μM and 0.106 μM, respectively. Notably, the Mn-PCN-222/ITO shows a good analytical response compared to 4-NBZ and 4-NP sensors reported in the literature (Tables S6, S7). Figure 3d establishes the simultaneous detection of NB and 4-NBZ with two well-resolved and distinct reduction peaks. On top of this, Mn-PCN-222/ITO detects NB and 4-NBZ mixtures in real water samples (tap and river water) with addition of different concentrations of NB (10 μM, 20 μM and 30 μM) and 4-NBZ (10 μM, 15 μM and 20 μM) at appreciable recoveries of 93.6 to 103.9% (Table S8). Meanwhile, the Mn-PCN-222/ITO shows highly linear responses to NB and 4-NBZ in the range of 0.5 to 100 μM with LODs of 0.027 μM and 0.029 μM, respectively. Similarly, the Mn-PCN-222/ITO also achieves simultaneous detection (1–100 μM) of 4-NP and 4-NBZ with LODs of 0.103 μM and 0.034 μM, respectively (Figure 3e). Moreover, a clear electrocatalytic response despite the co-existence of NB, 4-NBZ, 4-NP, suggests its usefulness in simultaneously detecting a set of target NACs (Figure S24). The proposed electrode could also recognize the number of nitro groups in an individual NAC analyte, confirmed by the two reduction peaks while detecting 1,3-DNB (Figure 3f).^[23]

For 1,3-DNB sensing, the excellent linearity observed across 0.08 to 100 μM with a LOD of 0.018 μM (based on peak b) establishes comparable sensing performances versus the hitherto reported electrodes (Table S9). Systematic studies on NACs detection demonstrate high efficiency of the Mn-PCN-222/ITO not only towards single-component systems, but also in binary and ternary systems (Figures 3 and S24).

To further reveal the sensory versatility of Mn-PCN-222/ITO, a series of voltammetric detections are performed on other analytes across different classes, *viz.* phenolics and quinone-hydroquinone, heavy metal ions, biological species, as well as the azo dyes. The sensing performances are detailed in Table 1 and Figures S25–S33. Upon comparing these against reported sensors, excellence of Mn-PCN-222/ITO becomes evident (Tables S10–16). Aligned with the demonstrated analyte-specific responses, Mn-PCN-222/ITO can also simultaneously detect mixtures of three analytes from three distinct classes: CT, 1,4-BZQ and AQDS (Figure S34); Cu^{2+} , $\text{Cr}_2\text{O}_7^{2-}$ and Cd^{2+} (Figure S35); AA and UA (Figure S36), suggesting it's high upside potentials to fabricate a multifaceted sensory device in binary and ternary systems.

Conclusion

In summary, a fast and facile modular assembly method is harnessed to cast porphyrinic Mn-PCN-222 film on the ITO glass. The resulting Mn-PCN-222/ITO demonstrates versatile voltammetric sensing of several analytes. The ordered incorporation of metalloporphyrin units as catalytic centers across a periodic and porous Mn-PCN-222 architecture facilitates the desired features of improved sensor design: a high-density of active sites, a large surface area, rapid analyte aggregation, mass transport and a sensitive response with a large linear range. All these features contribute to its benchmark

performance in sensing various analytes, *viz.*, nitroaromatics, phenolics, quinone-hydroquinone, heavy metal ions, biological species, as well as azo dyes. Sensitive detections with wide linear ranges and low LODs are obtained with Mn-PCN-222/ITO. The electrode shows high efficiency not only towards single substrates, but also retains its high performance in binary and ternary systems of increased complexity. An extension to more complex systems can be foreseen, upon conducting process/device engineering with this system. An optimal combination of selectivity, long-term stability, reproducibility and practicality of Mn-PCN-222/ITO is discovered. In essence, Mn-PCN-222/ITO not only turns out amenable to simple and efficient preparation methods, but also delivers excellent voltammetric detection performance and, therefore, holds great promise to design versatile electrochemical sensors in the future. Building upon the compositional modularity of M-PP-MOFs, varying intrinsic properties such as, pore environments, redox-potentials/windows for each (e.g., by choosing M properly or combining different M-PP-MOFs in one sensor device) paves the way for a number of related approaches, e.g., redox-potentials/windows are tuneable by an *à la carte* catalogue of metal nodes and this is likely to offer another dimension to the control of electrochemical properties of M-PP-MOF based voltammetric sensors.

Acknowledgements

Z.Y.Z. and S.J.H. are grateful for the PhD fellowship donated by the China Scholarship Council (CSC). W.L. and S.M. gratefully acknowledge the Alexander von Humboldt Foundation for their postdoctoral research fellowships. Z.Y.Z. is grateful to Katia Rodewald and Prof. Bernhard Rieger for providing the SEM data. We also appreciate the financial support from Deutsche Forschungsgemeinschaft (DFG) proj-

Table 1: Voltammetric detections of several analytes (belonging to different pollutant classes) on Mn-PCN-222/ITO.

Class	Analyte	Molecular structure ^[a]	Linear range [μM]	Limit of detection [μM]	Corresponding Figure
Phenolics and quinone-hydroquinone	Catechol (CT)		0.10–100	0.047	Figure S25
	1,4-benzoquinone (1,4-BZQ)		0.10–100	0.015	Figure S26
	Anthraquinone-2,6-disulfonate (AQDS)		0.06–100	0.020	Figure S27
Heavy metal ions	Cu^{2+}		0.06–100	0.013	Figure S28
	$\text{Cr}_2\text{O}_7^{2-}$		0.05–100	0.003	Figure S29
	Cd^{2+}		0.30–100	0.100	Figure S30
Biological species	Ascorbic acid (AA)		0.15–100	0.011	Figure S31
	Uric acid (UA)		0.08–100	0.017	Figure S32
Azo dyes	Methyl orange (MO)		0.07–100	0.009	Figure S33

[a] Color Scheme: C, grey; O, red; N, blue; H, white; S, gold; Cu, celeste; Cr, yellow and Cd, green.

ect MOFMOX (419949637) and by DFG Priority Program 1928 “Coordination Networks: Building Blocks for Functional Systems” (316376997). Open access funding enabled and organized by Projekt DEAL.

Conflict of Interest

The authors declare no conflict of interest.

Keywords: modular assembly · nitrobenzene detection · porphyrinic MOFs · sensors · thin film

- [1] a) S. Liu, C. Lai, X. Liu, B. Li, C. Zhang, L. Qin, D. Huang, H. Yi, M. Zhang, L. Li, W. Wang, X. Zhou, L. Chen, *Coord. Chem. Rev.* **2020**, *424*, 213520; b) D. W. Kimmel, G. LeBlanc, M. E. Meshievitz, D. E. Cliffler, *Anal. Chem.* **2012**, *84*, 685–707; c) B. J. Privett, J. H. Shin, M. H. Schoenfish, *Anal. Chem.* **2010**, *82*, 4723–4741.
- [2] a) A. J. Veloso, X. R. Cheng, K. Kerman, *Electrochemical Biosensors for Medical Applications* (Ed.: S. Higson), Woodhead Publishing, **2012**, pp. 3–40; b) M. M. Rodríguez-Delgado, G. S. Alemán Nava, J. M. Rodríguez Delgado, G. Dieck Assad, S. O. Martínez Chapa, D. Barceló, R. Parra, *TrAC Trends Anal. Chem.* **2015**, *74*, 21–45.
- [3] a) J. F. Rusling, S. L. Suib, *Adv. Mater.* **1994**, *6*, 922–930; b) N. Elgrishi, K. J. Rountree, B. D. McCarthy, E. S. Rountree, T. T. Eisenhart, J. L. Dempsey, *J. Chem. Educ.* **2018**, *95*, 197–206.
- [4] C. C. Wu, T. Yasukawa, H. Shiku, T. Matsue, *Sens. Actuators B* **2005**, *110*, 342–349.
- [5] a) H. Furukawa, K. E. Cordova, M. O’Keeffe, O. M. Yaghi, *Science* **2013**, *341*, 1230444; b) H. C. Zhou, J. R. Long, O. M. Yaghi, *Chem. Rev.* **2012**, *112*, 673–674; c) R. J. Kuppler, D. J. Timmons, Q. R. Fang, J. R. Li, T. A. Makal, M. D. Young, D. Yuan, D. Zhao, W. Zhuang, H. C. Zhou, *Coord. Chem. Rev.* **2009**, *253*, 3042–3066; d) S. T. Meek, J. A. Greathouse, M. D. Allendorf, *Adv. Mater.* **2011**, *23*, 249–267.
- [6] a) C. S. Liu, J. Li, H. Pang, *Coord. Chem. Rev.* **2020**, *410*, 213222; b) Y. Xu, Q. Li, H. Xue, H. Pang, *Coord. Chem. Rev.* **2018**, *376*, 292–318; c) S. Kempahanumakkagari, K. Vellingiri, A. Deep, E. E. Kwon, N. Bolan, K. H. Kim, *Coord. Chem. Rev.* **2018**, *357*, 105–129; d) S. Tajik, H. Beitollahi, F. Garkani Nejad, I. Sheikshoae, A. S. Nugraha, H. W. Jang, Y. Yamauchi, M. Shokouhimehr, *J. Mater. Chem. A* **2021**, *9*, 8195–8220.
- [7] a) R. Paollesse, S. Nardis, D. Monti, M. Stefanelli, C. Di Natale, *Chem. Rev.* **2017**, *117*, 2517–2583; b) J. Chen, Y. Zhu, S. Kaskel, *Angew. Chem. Int. Ed.* **2021**, *60*, 5010–5035; *Angew. Chem.* **2021**, *133*, 5064–5091; c) H. Lee, K. I. Hong, W.-D. Jang, *Coord. Chem. Rev.* **2018**, *354*, 46–73.
- [8] a) D. Feng, Z. Y. Gu, J. R. Li, H. L. Jiang, Z. Wei, H. C. Zhou, *Angew. Chem. Int. Ed.* **2012**, *51*, 10307–10310; *Angew. Chem.* **2012**, *124*, 10453–10456; b) Z. Zhou, S. Mukherjee, J. Warnan, W. Li, S. Wannapaiboon, S. Hou, K. Rodewald, B. Rieger, P. G. Weidler, C. Wöll, R. A. Fischer, *J. Mater. Chem. A* **2020**, *8*, 25941–25950.
- [9] a) Y. Chen, X. Sun, S. Biswas, Y. Xie, Y. Wang, X. Hu, *Biosens. Bioelectron.* **2019**, *141*, 111470; b) Y. Chen, W. Huang, C. Wang, X. Zhai, T. Zhang, Y. Wang, X. Hu, *ACS Sustainable Chem. Eng.* **2020**, *8*, 13226–13235; c) Y. Wang, L. Wang, H. Chen, X. Hu, S. Ma, *ACS Appl. Mater. Interfaces* **2016**, *8*, 18173–18181; d) S. Biswas, Y. Chen, Y. Xie, X. Sun, Y. Wang, *Anal. Chem.* **2020**, *92*, 4566–4572.
- [10] a) I. Stassen, N. Burtch, A. Talin, P. Falcaro, M. Allendorf, R. Ameloot, *Chem. Soc. Rev.* **2017**, *46*, 3185–3241; b) C. H. Su, C. W. Kung, T. H. Chang, H. C. Lu, K. C. Ho, Y. C. Liao, *J. Mater. Chem. A* **2016**, *4*, 11094–11102; c) P. M. Usov, B. Huffman, C. C. Epley, M. C. Kessinger, J. Zhu, W. A. Maza, A. J. Morris, *ACS Appl. Mater. Interfaces* **2017**, *9*, 33539–33543; d) A. L. Semrau, Z. Zhou, S. Mukherjee, M. Tu, W. Li, R. A. Fischer, *Langmuir* **2021**, *37*, 6847–6863.
- [11] a) G. Xu, T. Yamada, K. Otsubo, S. Sakaida, H. Kitagawa, *J. Am. Chem. Soc.* **2012**, *134*, 16524–16527; b) G. Xu, K. Otsubo, T. Yamada, S. Sakaida, H. Kitagawa, *J. Am. Chem. Soc.* **2013**, *135*, 7438–7441.
- [12] S. M. Yoon, J. H. Park, B. A. Grzybowski, *Angew. Chem. Int. Ed.* **2017**, *56*, 127–132; *Angew. Chem.* **2017**, *129*, 133–138.
- [13] a) Q. Xu, G. Zhan, Z. Zhang, T. Yong, X. Yang, L. Gan, *Theranostics* **2021**, *11*, 1937–1952; b) K. Yu, P. Puthiaraj, W. S. Ahn, *Appl. Catal. B* **2020**, *273*, 119059.
- [14] G. Granados-Oliveros, E. A. Páez Mozo, F. M. Ortega, C. Ferronato, J. M. Chovelon, *Appl. Catal. B* **2009**, *89*, 448–454.
- [15] K. S. Walton, R. Q. Snurr, *J. Am. Chem. Soc.* **2007**, *129*, 8552–8556.
- [16] a) P. S. Majumder, S. K. Gupta, *Water Res.* **2003**, *37*, 4331–4336; b) R. Emmanuel, C. Karuppiah, S. M. Chen, S. Palanisamy, S. Padmavathy, P. Prakash, *J. Hazard. Mater.* **2014**, *279*, 117–124; c) S. Kubendhiran, S. Sakthinathan, S. M. Chen, P. Tamizhdurai, K. Shanthi, C. Karuppiah, *J. Colloid Interface Sci.* **2017**, *497*, 207–216; d) C. Liu, X. Bo, L. Guo, *Sens. Actuators B* **2019**, *297*, 126741.
- [17] Y. G. Mourzina, A. Offenhäusser, *J. Electroanal. Chem.* **2020**, *866*, 114159.
- [18] a) A. Palma-Cando, U. Scherf, *ACS Appl. Mater. Interfaces* **2015**, *7*, 11127–11133; b) Z. Xue, H. Lian, C. Hu, Y. Feng, F. Zhang, X. Liu, X. Lu, *Aust. J. Chem.* **2014**, *67*, 796; c) X. Lu, Y. Quan, Z. Xue, B. Wu, H. Qi, D. Liu, *Colloids Surf. B* **2011**, *88*, 396–401.
- [19] a) C. W. Kung, T. H. Chang, L. Y. Chou, J. T. Hupp, O. K. Farha, K. C. Ho, *Chem. Commun.* **2015**, *51*, 2414–2417; b) S. R. Ahrenholtz, C. C. Epley, A. J. Morris, *J. Am. Chem. Soc.* **2014**, *136*, 2464–2472.
- [20] a) E. Laviron, *J. Electroanal. Chem.* **1974**, *52*, 355–393; b) M. B. Gholivand, M. Khodadadian, *Biosens. Bioelectron.* **2014**, *53*, 472–478; c) X. Ma, M. Chen, *Sens. Actuators B* **2015**, *215*, 445–450; d) S. Vinoth, P. M. Rajaitha, A. Pandikumar, *Compos. Sci. Technol.* **2020**, *195*, 108192.
- [21] a) S. Dong, G. Suo, N. Li, Z. Chen, L. Peng, Y. Fu, Q. Yang, T. Huang, *Sens. Actuators B* **2016**, *222*, 972–979; b) K. Kunpatee, S. Traipop, O. Chailapakul, S. Chuanuwatanakul, *Sens. Actuators B* **2020**, *314*, 128059.
- [22] N. Karikalalan, S. Kubendhiran, S. M. Chen, P. Sundaresan, R. Karthik, *J. Catal.* **2017**, *356*, 43–52.
- [23] a) Y. Sang, Y. Cui, Z. Li, W. Ye, H. Li, X. S. Zhao, P. Guo, *Sens. Actuators B* **2016**, *234*, 46–52; b) S. Pan, L. Wang, X. Chen, Y. Tang, Y. Chen, Y. Sun, X. Yang, P. Wan, *Electrochim. Acta* **2016**, *203*, 301–308.

Manuscript received: June 13, 2021

Revised manuscript received: July 13, 2021

Accepted manuscript online: July 14, 2021

Version of record online: August 6, 2021